Biochemical Journal (2021) **478** 1139–1157
https://doi.org/10.1042/BCJ20200628

PORTLAND PRESS

Research Article

Simultaneous targeting of CD44 and MMP9 catalytic and hemopexin domains as a therapeutic strategy

Gal Yosef[1,2], Hezi Hayun[1,2] and Niv Papo[1,2]

[1]Avram and Stella Goldstein-Goren Department of Biotechnology Engineering, Faculty of Engineering, Ben-Gurion University of the Negev, PO Box 653, Beer-Sheva 84105, Israel; [2]The National Institute for Biotechnology in the Negev, PO Box 653, Beer-Sheva 84105, Israel

Correspondence: Niv Papo (papo@bgu.ac.il)

OPEN ACCESS

Crosstalk of the oncogenic matrix metalloproteinase-9 (MMP9) and one of its ligands, CD44, involves cleavage of CD44 by the MMP9 catalytic domain, with the CD44–MMP9 interaction on the cell surface taking place through the MMP9 hemopexin domain (PEX). This interaction promotes cancer cell migration and invasiveness. In concert, MMP9-processed CD44 induces the expression of MMP9, which degrades ECM components and facilitates growth factor release and activation, cancer cell invasiveness, and metastasis. Since both MMP9 and CD44 contribute to cancer progression, we have developed a new strategy to fully block this neoplastic process by engineering a multi-specific inhibitor that simultaneously targets CD44 and both the catalytic and PEX domains of MMP9. Using a yeast surface display technology, we first obtained a high-affinity inhibitor for the MMP9 catalytic domain, which we termed C9, by modifying a natural non-specific MMP inhibitor, N-TIMP2. We then conjugated C9 via a flexible linker to PEX, thereby creating a multi-specific inhibitor (C9-PEX) that simultaneously targets the MMP9 catalytic and PEX domains and CD44. It is likely that, via its co-localization with CD44, C9-PEX may compete with MMP9 localization on the cell surface, thereby inhibiting MMP9 catalytic activity, reducing MMP9 cellular levels, interfering with MMP9 homodimerization, and reducing the activation of downstream MAPK/ERK pathway signaling. The developed platform could be extended to other oncogenic MMPs as well as to other important target proteins, thereby offering great promise for creating novel multi-specific therapeutics for cancer and other diseases.

Introduction

The cell-surface glycoprotein CD44 is abundantly expressed throughout the body [1] in both health and disease, but its expression in cancer cells is particularly high [2]. CD44 is therefore regarded as a cancer biomarker for a variety of cancer types, including ovarian, head and neck, and gastric cancers [3–5], with its overexpression serving as a predictor for poor prognosis in cancer patients [6,7]. When phosphorylated at Ser325, positioned on its cytoplasmic tail, CD44 can serve as a docking transmembrane receptor on the cancer cell surface for one of its ligands, matrix metalloproteinase-9 (MMP9) [8]. This multi-domain protease consists of a signal peptide, a cysteine switch motif, a propeptide, a fibronectin type II motif, a hinge region, and — importantly for this study — a catalytic domain and a hemopexin (PEX) domain [9]. It is known that the interaction between CD44 and MMP9 is selective and does not necessarily occur in all cells that express the two proteins [10,11]. It is, therefore, possible that the CD44–MMP9 interaction is specific for cancer cells, as has been shown, for example, in B-cell chronic lymphocytic leukemia (B-CLL) compared with normal B cells (for which there is no interaction) [11]. It has also been reported that the CD44–MMP9 interaction increases invasiveness [12] and leads to the activation of MAPK signaling, which results in cancer cell

Received: 10 August 2020
Revised: 9 February 2021
Accepted: 17 February 2021

Accepted Manuscript online: 17 February 2021
Version of Record published: 12 March 2021

Biochemical Journal (2021) 478 1139–1157
https://doi.org/10.1042/BCJ20200628

migration [13]. In carcinoma cells, digestion of CD44 — in a process involving sequential proteolytic cleavage by MMP9 and γ-secretase — produces an intracytoplasmic domain ($CD44_{ICD}$) cleavage product that translocates into the cell nucleus and promotes MMP9 gene expression [14–16]. Finally, it is known that upon its secretion from cells as a stable, inactive zymogen (i.e. pro-MMP9) and subsequent activation by proteolytic enzymes, catalytically active MMP9 degrades extracellular matrix (ECM) components, leading to the release and activation of growth factors and the promotion of invasiveness and metastasis of many cancers, such as breast, ovarian and bladder cancers [18–24].

A well-established mode of interaction of CD44 with MMP9 takes place through the PEX domain of MMP9. The resulting CD44/MMP9 complex formed on the cell surface induces the activation of transforming growth factor beta (TGF-β), ECM degradation, and the migration, invasion and metastasis of cancer cells, as has been reported for breast and prostate cancers [11,12,18,25,26]. Enhancement of ECM degradation and cancer cell invasiveness is therefore the outcome of both MMP9 proteolytic activity [17] and interaction between MMP9 and CD44 via the PEX domain of MMP9 [11,18,25]. Importantly, CD44 can also interact with MMP9 in the form of a homodimer, in which two MMP9 polypeptides are non-covalently bound through blades IV of the monomer PEX domains [27]. In this case, CD44 interacts with the MMP9 homodimer through blades I of the PEX domains, with the interaction leading to extracellular signal-regulated kinase (ERK) phosphorylation and hence to the promotion of cell migration [13,27].

In light of the above, both CD44 and MMP9 constitute attractive targets for cancer therapeutics, and many attempts have been made to generate inhibitors for each of them separately. Despite the development of such mono-specific inhibitors, including antibodies [28–32], peptides [32,33] and small molecules [34,35], there is still no clinically available treatment that rests on targeting either CD44 or MMP9. In a different type of strategy, attempts have been made to inhibit cancer cell migration by targeting the PEX domain of MMP9 with peptides extracted from the PEX domain or with small molecules [27,36–38], but the results, although promising, have not yielded a clinically applicable product. The path forward would therefore appear to lie in interrupting the cross-talk between CD44 and MMP9 that leads to the migration and invasiveness of cancer cells, namely, in targeting the two molecules simultaneously [12,13]. Nonetheless, no attempts have been made to simultaneously inhibit MMP9 catalytic activity and its interaction with CD44 (mediated through the PEX domain of MMP9). Our working hypothesis for this study was therefore that targeting the CD44/MMP9 axis, i.e. CD44 and both the MMP9 catalytic domain ($MMP9_{CAT}$) and the MMP9 PEX domain, with a multi-specific inhibitor would generate a potent inhibitor. Such a strategy would be required to: (i) enhance the local concentration of the multi-specific inhibitor near the desired protein targets (since MMP9 and CD44 are co-localized on the cell surface), (ii) provide synergistic inhibition of the CD44/MMP9 complex compared with inhibition of each target alone, and (iii) exhibit enhanced specificity towards cancer cells in which the MMP9 and CD44 targets are co-localized and expressed.

As a starting point for developing such a multi-pronged inhibitor, tissue inhibitors of matrix metalloproteinases 1–4 (TIMP1–4) were judged to be suitable candidates, since these four homologous mammalian TIMPs are natural inhibitors of all 28 known MMP family members [19]. Among these candidates, the choice of TIMP2 was governed by the following considerations: TIMP1–4 show 40–50% sequence identity with one another and exhibit slightly different preferences for the different MMPs [39], but TIMP2 binds to MMP9 more strongly than to other MMPs [40]. In addition, while MMP9 is associated with cancer progression and metastasis [23], several other MMPs are considered to be 'protective' against cancer, and it was therefore necessary to choose an inhibitor that would specifically target MMP9 [41,42]. Engineering such selective targeting of an MMP by a TIMPs is, however, challenging, since all MMPs share a highly homologous catalytic site [43,44].

TIMP2 is composed of two domains, an N-terminal domain (N-TIMP2), which is responsible for inhibition of MMPs, and a C-terminal domain (C-TIMP2), which takes part in MMP2-dependent activation of MMP9 — in an undesired reaction sequence that contributes to cancer progression [45–47]. N-TIMP2 inhibits the activity of MMPs mainly via its interface residue Cys1, which chelates the catalytic zinc atom of MMPs in a process that expels the Zn-bound water molecule that is required for peptide bond hydrolysis [9,39]. Other interface positions in N-TIMP2 are considered 'cold-spots', i.e. tolerant to mutagenesis, and can be optimized for enhanced binding specificity towards a specific MMP [9,39,40]. In the current study, we exploited this tolerance to mutagenesis to generate a library of N-TIMP2 variants — with each variant containing seven random mutations at cold spot positions (namely, positions 4, 35, 38, 68, 71, 97 and 99) — and screened this library to select high-affinity binders to MMP9. One of the selected N-TIMP2 variants, which we designated C9, exhibited superior MMP9 inhibition in comparison with the parental wild-type N-TIMP2 ($N\text{-}TIMP2_{WT}$).

To enhance the specificity and the inhibition potency of C9 towards MMP9, we then engineered a multi-specific adduct, designated here as C9-PEX, which is composed of C9 conjugated (at its C-terminus) to the PEX domain of MMP9 via a flexible linker (Supplementary Figure S1). In keeping with our working hypothesis, we used the multi-specific C9-PEX adduct to target both MMP9 (via the interaction of the C9 and PEX domains of the adduct with the catalytic and PEX domains of MMP9) and its co-localized receptor CD44 (via the interaction of the PEX domain of the adduct with CD44). We posited that the adduct would exhibit enhanced potency and specificity towards MMP9, particularly since the PEX domain of MMP9 has low similarity to the PEX domains of other MMPs [38]. The present study showed that, indeed, the multi-specific C9-PEX protein adduct both inhibited MMP9 catalytic activity and served as an antagonist for CD44, the latter via C9-PEX/CD44 co-localization and binding, which presumably blocks the MMP9/CD44 interaction. Moreover, the results of the study suggest tight-binding between C9-PEX and MMP9, leading to a reduced quantity of MMP9 homodimers and reduced ERK phosphorylation, both of which may result in attenuated cancer cell migration.

Materials and methods

Screening of the N-TIMP2 focused library

A focused N-TIMP2 library with random mutations at seven binding interface positions (i.e. 4, 35, 38, 68, 71, 97, 99) (PDB: 1BUV) [48] of the N-TIMP2 gene was purchased from GenScript (Piscataway, NJ). The library had been prepared with NNS (where N represents A, C, T or G nucleotides, and S represents C or G) degenerate codons that were used to mutate the N-TIMP2$_{WT}$ gene at the above-mentioned positions. In our laboratory, the library was expressed in a yeast surface display (YSD) system using the pCHA vector, which was introduced into *Saccharomyces cerevisiae* EBY100 (both pCHA and EBY100 were obtained from Dane Wittrup, MIT), as previously described [40]. A library size of 8×10^6 clones was confirmed by performing serial dilutions on selective SDCAA plates (2% dextrose, 0.67% yeast nitrogen base, 0.5% Bacto™ Casamino acids, 1.47% sodium citrate, 0.429% citric acid monohydrate, pH 4.5, 1.5% agar). The yeast-displayed N-TIMP2 library was grown in a selective medium [yeast nitrogen base (6.7 g/L), Na_2HPO_4 (5.4 g/L), $NaH_2PO_4 \bullet H_2O$ (8.56 g/L), dextrose (20 g/L), Bacto Casamino acids (5 g/L)] and induced for expression with galactose (20 g/L), as previously described [49].

The yeast cells (1×10^6–80×10^6) were FACS (fluorescence-activated cell sorting) sorted in multiple rounds — each round against a different concentration of soluble, fluorescently labeled MMP9$_{CAT}$, as previously described with some modifications [40]. Briefly, yeast cells were labeled with a 1 : 50 dilution of mouse anti-cMyc antibody (Abcam, Cambridge, U.K.) in MMP buffer [50 mM Tris, pH7.5, 100 mM NaCl, 5 mM $CaCl_2$ and 1% bovine serum albumin (BSA)] for 1 h at room temperature. Cells were washed and resuspended in ice-cold MMP buffer containing DyLight™ 650-labeled MMP9$_{CAT}$ and a 1 : 50 dilution of phycoerythrin (PE)-conjugated goat anti-mouse-IgY (Merck Millipore, MA, U.S.A.). After 30 min on ice, the cells were washed with MMP buffer and sorted using a FACS Aria III [Ilse Katz Institute for Nanoscale Science and Technology, Ben-Gurion University of the Negev (BGU)]. In the expression sort, only yeast cells expressing intact N-TIMP2 proteins were selected (using the mouse anti-cMyc antibody). For the subsequent MMP9$_{CAT}$ affinity sorts, the concentrations of MMP9$_{CAT}$ that were added to the yeast cells were decreased with each sort, as follows: 500 nM (sorts 1, 2), 200 nM (sort 3) and 50 nM (sort 4). In each MMP9$_{CAT}$ sort, 1–2% of the yeast high affinity (relative to expression) cell population were collected using a diagonal sorting gate. After each sort round, the yeast plasmid DNA was purified using a Zymoprep™ Yeast Plasmid Miniprep I kit (ZymoResearch, CA, U.S.A.). Then, the plasmid was transformed into electro-competent *Escherichia coli* and grown overnight on ampicillin (100 μg/ml) LB-agar plates. Thereafter, 15–20 colonies were transferred to an ampicillin (100 μg/ml)-LB culture medium and grown overnight at 37°C. The plasmid was extracted from the bacteria using a HiYield plasmid mini kit (RBC Bioscience, New Taipei City, Taiwan) and was then sequenced (Genetics Unit, NIBN, BGU, Israel).

For the YSD-based affinity saturation titrations, the same labeling process was utilized, and the binding of the YSD N-TIMP2$_{WT}$ and C9 variants to MMP9$_{CAT}$ was determined at MMP9$_{CAT}$ concentrations of 2, 3.9, 7.8, 15.6, 31.3, 62.5, 125, 250 and 500 nM and 1 μM. When needed, the reaction volume was increased to prevent ligand depletion. For each clone, the value of the fluorescence signal of each measurement at each concentration was normalized to the value showing the highest binding. A nonlinear binding fit was implemented using GraphPad Prism (GraphPad software, CA, U.S.A.). The apparent K_D value for each protein was calculated

Biochemical Journal (2021) 478 1139–1157
https://doi.org/10.1042/BCJ20200628

using this fit and the equation for one-site specific binding (eqn 1).

$$Y = \frac{B_{max} \cdot X}{K_D + X} \quad (1)$$

where Y — specific binding, X — ligand concentration, B_{max} — maximum specific binding, and K_D — equilibrium dissociation constant.

Generation of the multi-specific C9-PEX adduct and mono-specific CD44-binding proteins

The C9-PEX gene comprising C9 fused to the PEX domain of MMP9 (positions 506–707) [50] through a flexible linker (S(GGGGS)$_3$3) was purchased from Genscript (NJ, U.S.A.). Two mono-specific variant genes, namely, PEX of MMP9 and A-C9-PEX (which has an alanine residue appended to the N-terminus of C9-PEX and binds only to CD44), were generated for protein production in the methylotrophic yeast strain X-33 *Pichia pastoris* using PCR and the C9-PEX gene as a template. The following primers were used to generate the genes for the mono-specific proteins:

PEX Fwd: 5′-GGTATCTCTCGAGAAAAGAACAGTGCCCTTGAGTCCC-3′
A-C9-PEX Fwd: 5′-GGTATCTCTCGAGAAAAGAGCATGCTCCTGTATGCCCGTG-3′
PEX and A-C9-PEX Rev: 5′-GCTGGCGGCCGCGTCTTCAGGGCACTGTAAGATGTC-3′

Production and purification of soluble proteins

The human MMP9 catalytic domain ($MMP9_{CAT}$) lacking the fibronectin-like domain (residues 107–215 and 391–443) [51] was a generous gift from Irit Sagi (Weizmann Institute of Science, Rehovot, Israel). Purified $MMP9_{CAT}$ was labeled with DyLight-650 (Thermo Fisher, MA, U.S.A.), as previously described [40].

N-$TIMP2_{WT}$, C9, C9-PEX, A-C9-PEX, and PEX proteins were produced in soluble form in *P. pastoris* strain X-33 according to the pPICZα protocol (Invitrogen, CA, U.S.A.), as previously described with some modifications [40]. Briefly, N-$TIMP2_{WT}$, C9, C9-PEX, A-C9-PEX, and PEX genes were cloned into the pPICZαA vector for expression in *P. pastoris* strain X-33. Proteins were prepared with both c-Myc and 6× His tags at the C-terminus for protein detection and purification, respectively. The proteins were purified from the yeast growth medium by affinity column chromatography using nickel nitrilotriacetic acid-Sepharose beads (Invitrogen) equilibrated in a mixture of 50 mM Tris, pH 7.5, 300 mM NaCl and 10 mM imidazole, and eluted with a mixture of 50 mM Tris, pH 7.5, 300 mM NaCl and 300 mM imidazole. Thereafter, separation on a gel filtration Superdex 75 column (GE Healthcare, PA, U.S.A.), equilibrated in 50 mM Tris pH 7.5, 300 mM NaCl and 5 mM $CaCl_2$ at a flow rate of 0.8 ml/min on an ÄKTA pure instrument (GE Healthcare), was performed. Protein size was verified by SDS–PAGE and mass spectrometry analysis (Ilse Katz Institute for Nanoscale Science and Technology, BGU, Israel). Protein concentrations were determined by UV-Vis absorbance at 280 nm, using a NanoDrop Spectrophotometer (ε_{280} of 13 325 M^{-1} cm^{-1} for N-$TIMP2_{WT}$ and C9, 52 870 M^{-1} cm^{-1} for C9-PEX and A-C9-PEX, and 39 545 M^{-1} cm^{-1} for PEX). Yields of all purified proteins were 2–21 mg/L.

MMP9 inhibition studies

The inhibition constant (*Ki*) was determined as previously described [52]. The inhibition of the catalytic activity of MMP9 (0.325 nM) against the fluorogenic substrate Mca-Pro-Leu-Gly-Leu-Dpa-Ala-Arg-NH_2·TFA (7.5 μM, Merck Millipore) was determined using N-$TIMP2_{WT}$ at 0.0625–1 nM, C9 at 0.031–1 nM, and C9-PEX at 0.047–1 nM. *Ki* was calculated according to Morrison's equation (eqn 2), the classic competitive inhibition equation for tight binding, by using Prism (GraphPad Software). Mean values of *Ki* ± standard deviation (SD) were obtained from three independent experiments.

$$\frac{V_i}{V_o} = 1 - \frac{([E] + [I] + Ki^{app}) - \sqrt{([E] + [I] + Ki^{app})^2 - 4[E][I]}}{2[E]} \quad (2)$$

where V_i — enzyme velocity in the presence of inhibitor, V_0 — enzyme velocity in the absence of inhibitor, E — enzyme concentration, I — inhibitor concentration, S — substrate concentration, K_M — Michaelis-Menten

constant, and Ki^{app} — the apparent inhibition constant, which is given by:

$$Ki^{app} = Ki\left(1 + \frac{[S]}{K_m}\right)$$

where Ki — inhibition constant.

Cell culture

Cells of the MCF-7 human breast cancer cell line (a generous gift from Dan Levy, BGU) were maintained in Dulbecco's modified Eagle's medium (DMEM; Biological Industries, Beit-Haemek, Israel) supplemented with 10% fetal bovine serum (Thermo Fisher, MA, U.S.A.), 1% L-glutamine (Biological Industries) and 1% penicillin/streptomycin (Biological Industries). HT1080 cells (ATCC CCL-121), endogenously expressing both MMP9 and MMP2, were maintained in Roswell Park Memorial Institute (RPMI) 1640 medium with L-glutamine (Biological Industries) supplemented with 10% fetal bovine serum and 1% penicillin/streptomycin. All cells were maintained at 37°C under 5% CO_2.

Generation of a stable MCF7-MMP9 cell line

For generating stable MCF-7 cells expressing MMP9 (designated MCF7-MMP9), MCF-7 cells (10^5) were seeded in the wells of a six-well plate and incubated in DMEM medium supplemented with serum for 24 h at 37°C under 5% CO_2. The cells were then transfected with a pCMV MMP9 plasmid (Sino Biological, Beijing, China) using Lipofectamine 3000 (Thermo Fisher) according to the manufacturer's instructions. Forty-eight hours post-transfection, the cells were treated with 150 μg/ml of hygromycin (Thermo Fisher), followed by an incubation of 4 weeks at 37°C under 5% CO_2. The expression of MMP9 in MCF7-MMP9 transfected cells and MCF-7 control cells was determined using a gelatin zymography assay, as described below [52]. CD44 expression was evaluated using FITC anti-human CD44 antibody (BioLegend, CA, U.S.A.) and was detected using a BD Accuri C6 flow cytometer (BD Biosciences, CA, U.S.A.).

Gelatin zymography assay

The gelatinolytic inhibitory activity of the N-TIMP2 proteins was determined in a gelatinase zymography assay, as previously described [53], with some modifications, as follows. The cells — either MCF7-MMP9 or HT1080 — at a quantity of 10^5 were grown to 70–80% confluence in the medium (DMEM or RPMI 1640, respectively) supplemented with serum. The medium was then replaced with serum-free medium (DMEM or RPMI 1640, respectively), and the cells were incubated for 24 h or 72 h, respectively, at 37°C under 5% CO_2. The growth medium, containing the secreted MMP9 (and MMP2 for HT1080), was collected and centrifuged for 5 min at 10,000***g***. The supernatant was then loaded onto gelatin SDS–PAGE, washed for 1 h in 2.5% Triton X-100, and incubated overnight in a developer buffer (50 mM Tris, pH 7.4, 10 mM $CaCl_2$, and 0.02% NaN_3), containing 150 nM for MCF7-MMP9, or 50 nM for HT1080, of each N-TIMP2 protein at 37°C, as previously described [40]. Gels were stained with SimplyBlue™ SafeStain (Thermo Fisher) and captured with MiniBIS Pro (DNR Bio-Imaging Systems, Neve Yamin, Israel). The intensity of the white bands was quantified using ImageJ. A gelatinase zymography experiment was also performed using 1 ng recombinant, full-length MMP9 (BioLegend), preactivated with 1 mM 4-aminophenylmercuric acetate (APMA) according to the manufacturer's protocol. The gelatinolytic inhibitory activity in MCF7-MMP9 cells incubated for 24 h with 1 μM C9-PEX or monospecific controls was also determined using MCF7-MMP9 cell lysates. The treated cells were lysed using a zymography sample buffer with 30 min incubation at 37°C, and the lysate was loaded onto gelatin SDS–PAGE prior to analysis as described above.

CD44 and C9-PEX co-localization assay

MCF7-MMP9 cells (2.5×10^4) were seeded on an eight-well chamber slide and incubated overnight at 37°C under 5% CO_2. Thereafter, cells were washed three times with PBSA (0.1% BSA in PBS), and incubated for 2 h with 10 μl of FITC anti-human CD44 antibody and 100 μg of DyLight 647-labeled C9-PEX. Hoechst stain (1 μg, Invitrogen) was added to the cells 10 min before analysis. Cells were washed three times with PBSA, and then analyzed with an FV1000 confocal fluorescence microscope (Olympus, PA, U.S.A.).

Biochemical Journal (2021) 478 1139–1157
https://doi.org/10.1042/BCJ20200628

Determination of secreted MMP9 levels

The quantities of secreted MMP9 were assessed using a gelatin zymography assay, as previously described [52]. Human MCF7-MMP9 or HT1080 cells (2×10^4) were grown overnight on a 96-well plate at 37°C under 5% CO_2. Thereafter, the cells were treated for 24 h with 1 μM N-TIMP2$_{WT}$, C9, C9-PEX, PEX, A-C9-PEX, C9 and PEX together, or C9 and A-C9-PEX together in the relevant serum-free medium. The cell medium was collected, centrifuged for 5 min at 10,000***g***, and subjected to a gelatin zymography assay, as described above. To monitor the effect of different concentrations of C9-PEX on MMP9, the same process was performed using different concentrations of C9-PEX (i.e. 10 μM, 5 μM, 2 μM, 1 μM, 100 nM and 10 nM) in the relevant serum-free medium. In addition, the expression of endogenous CD44 on the HT1080 cell membrane was verified using FITC anti-human CD44 antibody (BioLegend) and was detected using a BD Accuri C6 flow cytometer (BD Biosciences).

Cell viability assay

MCF7-MMP9 cells (1.2×10^4) were grown overnight at 37°C under 5% CO_2 on a 96-well plate. Thereafter, the cells were treated for 24 h with different concentrations of C9-PEX, namely, 10 μM, 5 μM, 2 μM, 1 μM, 100 nM or 10 nM, in serum-free medium. XTT reagent (Biological Industries, Israel) was added according to the manufacturer's instructions, and the absorbance was measured after 2 h at wavelengths of 450 nm and 690 nm.

Reduction in the quantities of MMP9 monomers and dimers

MCF7-MMP9 cells were grown at 37°C under 5% CO_2 to 70–80% confluence. Thereafter, the cell medium was replaced with serum-free DMEM medium, and the cells were incubated with that medium for 48 h. The cell medium (containing the secreted MMP9) was then collected and centrifuged for 5 min at 10,000***g***. The supernatant (100 μl) was incubated at 37°C for 24 h with 5 μM, 1 μM or 500 nM C9-PEX, 5 μM A-C9-PEX, or 5 μM C9 and then subjected to a zymography assay (as described above). As a high concentration of MMP9 homodimers was required for visualization, the cell medium was concentrated by 36-fold, using a 5 kDa cut-off Vivaspin (GE Healthcare). The concentrated medium (100 μl) was incubated at 37°C for 24 h with 5 μM C9-PEX, A-C9-PEX, C9, or a mix of A-C9-PEX and C9, and subjected to a zymography assay (as described above).

Phosphorylation assay

To evaluate the effect of MMP9 on ERK1/2 phosphorylation, MCF-7 or MCF7-MMP9 cells (3×10^5) were grown overnight at 37°C under 5% CO_2 on a six-well plate. Thereafter, the cells were washed three times with PBS, and divided into three groups, with each group being treated for 10 min with a different type of medium: serum-free DMEM medium, serum-free DMEM medium collected after 24 h of incubation with MCF-7 cells, or serum-free DMEM medium collected after 24 h of incubation with MCF7-MMP9 cells. To assess the effect of the proteins on ERK1/2 phosphorylation, two different concentrations of C9-PEX, C9 and Ala-C9-PEX (i.e. 5 μM and 500 nM) in serum-free DMEM medium (collected from MCF7-MMP9 cells after 24 hr incubation) were added to the cells for 10 min. Thereafter, the cells were washed three times with ice-cold PBS and then exposed to a lysis buffer (0.5% deoxycholate, 25 mM NaF, 10 mM $NaPO_4$, 1 mM sodium orthovanadate, 5 mM EDTA pH 7.4, 5 mM EGTA pH 7.4, 100 mM NaCl, 2% Triton X-100, protease inhibitor cocktail). The cells were then scraped from the culture plate wells, and the lysates were clarified by centrifugation (13 000 rpm for 30 min at 4°C). Lysate samples were loaded onto three 10% SDS–PAGE systems and transferred to three PVDF membranes (Bio-Rad, CA, U.S.A.). Blots were blocked with 5% BSA in TBST (50 mM Tris–HCl, pH 7.4, 150 mM NaCl, 0.1% Tween 20) for 1 h at room temperature and then incubated overnight at 4°C with a 1 : 2000 dilution of rabbit anti-MAP kinase pAb (Sigma–Aldrich, MO, U.S.A.), a 1 : 2000 dilution of mouse anti-MAP kinase activated mAb (Sigma–Aldrich), or a 1 : 1000 dilution of anti-β-actin pAb (Cell Signaling Technology, MA, U.S.A.). Membranes were washed three times with TBST and incubated for 1 h at room temperature with a 1 : 2000 dilution of HRP-linked anti-rabbit antibody (Cell Signaling Technology) or HRP-linked anti-mouse antibody (Cell Signaling Technology). Membranes were then washed again three times with TBST, and band intensities, representing the pERK1/2, ERK1/2 and β-actin, were visualized and quantified using chemiluminescence (ECL, Biological Industries) and ImageJ software, respectively. The intensities of the

phosphorylated ERK1/2 bands measured by ImageJ were normalized to the expression of total ERK1/2 of each experiment, and this value was subsequently normalized to the total quantity of β-actin for each sample.

Statistical analysis

All assay results are reported as means (±SD) of three or four biological repetitions (the number of repetitions for each experiment is given in the figure legends). One-way ANOVA with Dunnett's multiple comparison to the untreated controls was utilized for the statistical analysis.

Results

Construction and screening of the N-TIMP2 focused library

To generate high-affinity inhibitors to MMP9, an N-TIMP2 YSD focused library (designated N-TIMP2$_{LIB}$) was designed such that positions 4, 35, 38, 68, 71, 97 and 99 were randomly mutagenized to all 20 amino acids by using degenerate codons. To isolate N-TIMP2 variants with high-affinity for MMP9$_{CAT}$ (residues 107–215, 391–443) [51,54], five rounds of FACS were performed such that the first round was used for selecting all high-expressing variants (designated expression sort, ES), and the four additional sorts (sorts 1–4) were used for affinity enrichment towards soluble MMP9$_{CAT}$ (Figure 1). In each round of affinity sorting, the MMP9$_{CAT}$ concentration was reduced, and the fraction of cells having a high affinity to MMP9$_{CAT}$ was enriched (Figure 1B). Twelve N-TIMP2 variants were identified and isolated after sort 4; of these, one of the variants, designated C9, was chosen (on the basis of its strong binding to MMP9$_{CAT}$ in the YSD format, Supplementary Figure S2) for further purification as a soluble protein. The binding of C9 and the parental N-TIMP2$_{WT}$ proteins, displayed on the yeast surface, was determined for different concentrations of MMP9$_{CAT}$ by using flow cytometry. The resulting MMP9$_{CAT}$ affinity titration curves generated for C9 and N-TIMP2$_{WT}$ gave calculated apparent K_D values of 7.34 ± 0.66 nM and 57.09 ± 5.69 nM, respectively (Supplementary Figure S3), values that serve to highlight the improvement in C9 binding to MMP9 in comparison with the parental N-TIMP2$_{WT}$.

Generation of mono- and multi-specific binders to MMP9 and CD44

To further enhance the specificity and potency of the N-TIMP2-based inhibitor, C9 was engineered to produce a multi-specific protein adduct that would bind to both MMP9 and CD44 (known to be co-localized and to act in concert to mediate the invasiveness of breast and prostate cancer cells [8,12,13], inter alia). The multi-specific protein adduct – designated C9-PEX — was engineered by fusing the C-terminus of C9 to the N-terminus of the MMP9 PEX domain via a flexible S(GGGGS)$_3$ linker. An important consideration in

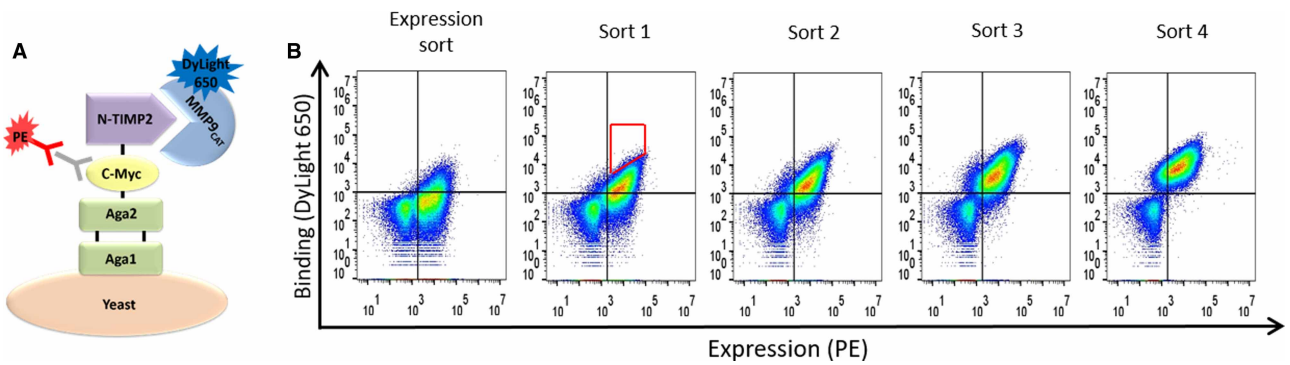

Figure 1. Affinity maturation by YSD.

(**A**) Schematic representation of the YSD system. The N-TIMP2 library (N-TIMP2$_{LIB}$) fused to Aga2p expressed in yeast was disulfide-bonded to Aga1p covalently bound to the yeast cell wall. Expression of the N-TIMP2$_{LIB}$ variants was detected by targeting the c-Myc epitope tag, expressed on the C-terminus of each protein variant, with an antibody labeled with phycoerythrin (PE). The binding to MMP9$_{CAT}$ was detected by the fluorescent signal of DyLight 650-labeled MMP9$_{CAT}$. (**B**) Flow cytometry analysis of the sorted library tested against 5 nM MMP9$_{CAT}$. In the expression sort, the parental N-TIMP2$_{LIB}$-expressing cell population was sorted. In each of the affinity sorts 1–4, the MMP9$_{CAT}$ high affinity population was collected (~2% of the entire population, shown only for sort 1 — red gate). Affinity enrichment of the library towards MMP9$_{CAT}$ was thus obtained in the sorting process.

Biochemical Journal (2021) **478** 1139–1157
https://doi.org/10.1042/BCJ20200628

Table 1 Inhibition constants (*Ki*) of N-TIMP2 proteins with MMP9

Protein	*Ki* (nM)	Fold increase $\left(\frac{ki\ \text{protein}}{ki\ \text{WT}}\right)^{1}$
N-TIMP2$_{WT}$	0.1880 ± 0.0057	1
C9	0.0141 ± 0.0010	13.33
C9-PEX	0.0777 ± 0.0016	2.42

[1]Fold increase was calculated as the ratio of *Ki* of the protein to *Ki* of N-TIMP2$_{WT}$.

engineering this adduct was the necessity to keep the N-terminus domain of C9 free, since this domain is essential for the inhibition of MMP catalytic activity [55]. In addition to the multi-specific C9-PEX inhibitor, two mono-specific controls that bind to CD44, but not to MMP9$_{CAT}$, were chosen, namely, the MMP9 PEX domain itself and an adduct designated A-C9-PEX, in which an alanine residue was appended to the N-terminus of C9 in the C9-PEX adduct. The design of A-C9-PEX was based on a report that addition of an alanine residue to TIMP2 abolished its MMP inhibition ability [56]. C9 served as the mono-specific inhibitor for MMP9. The above multi-specific and mono-specific variants and N-TIMP2$_{WT}$ were produced as purified proteins with a free N-terminus (which is crucial for MMP inhibition), but with histidine and c-Myc tags on the C-terminus (Supplementary Figure S4). The ability of the inhibitors to inhibit the catalytic activity of the full-length MMP9 protease on a fluorescent peptide substrate, as reflected by the *Ki* values (Table 1 and Figure 2), was found to be (from highest to lowest): C9 > C9-PEX > N-TIMP2$_{WT}$. These results for the *Ki* values, which are in agreement with the apparent K_D values obtained from the YSD titration curves (Supplementary Figure S3), demonstrate the improvement in the MMP9 inhibition (and binding) potency of the engineered C9 protein compared with N-TIMP2$_{WT}$. We note that it was important to achieve this improvement in affinity/inhibition towards MMP9 because, as we observed, there was a need to compensate for the reduction in the C9 inhibitory activity of C9-PEX due to its fusion with the PEX domain (Table 1 and Figure 2). The MMP9 PEX domain itself and the adduct designated A-C9-PEX, both of which serve as CD44 mono-specific controls, were used in experiments described further on in the manuscript.

N-TIMP2 proteins inhibit the gelatinolytic activity of MMP9

To test the inhibitory activity of the proteins in a cellular system, MCF-7 cells stably transfected with MMP9 (MCF7-MMP9) were generated, and expression of MMP9 and CD44 was verified in a zymography assay and by flow cytometry with an anti-CD44 antibody, respectively (Supplementary Figure S5). To test the inhibitory activity of N-TIMP2 proteins on the gelatinolytic behavior of MMP9, a gelatin zymography assay was performed on pre-activated recombinant, full-length MMP9 (MMP9$_{FL}$) and MMP9 secreted from MCF7-MMP9 cells. In this assay, pre-activated MMP9$_{FL}$ or the MCF7-MMP9 cell medium (containing the secreted MMP9) was loaded onto gelatin SDS–PAGE, followed by incubation of the gels with 50 nM or 150 nM of the different N-TIMP2 proteins, namely, N-TIMP2$_{WT}$, C9 and C9-PEX. The gelatinolytic activity of MMP9 was visualized

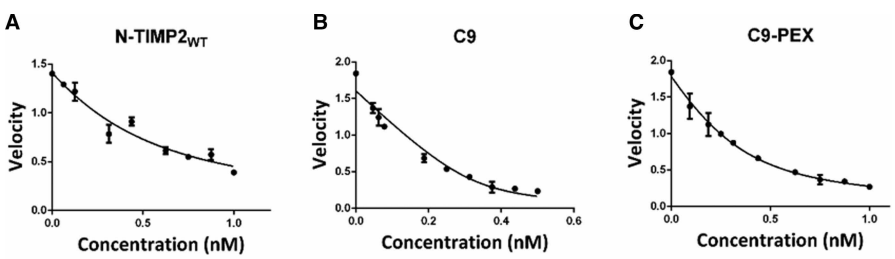

Figure 2. Substrate degradation velocity by C9 and C9-PEX vs N-TIMP2$_{WT}$.
Substrate degradation velocity at different concentrations of inhibitors for (**A**) N-TIMP2$_{WT}$ (0–1 nM), (**B**) C9 (0–0.5 nM), and (**C**) C9-PEX (0–1 nM). The substrate degradation velocity was fitted to Morrison's equation (eqn 2) to obtain *Ki* values. Error bars represent SD; $n = 3$.

Biochemical Journal (2021) **478** 1139–1157
https://doi.org/10.1042/BCJ20200628

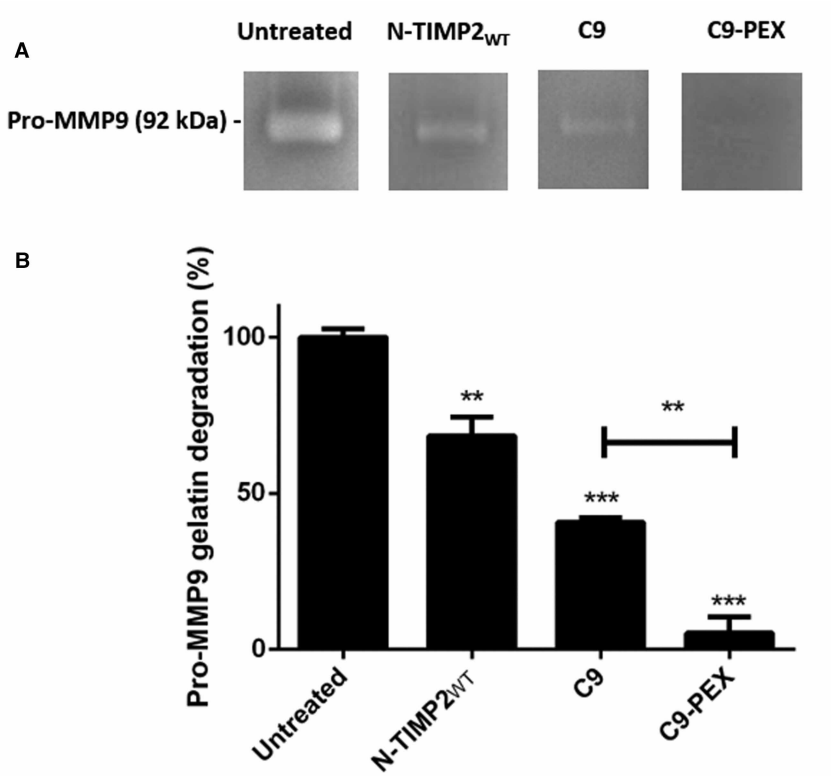

Figure 3. N-TIMP2 proteins inhibit gelatin degradation by MMP9 secreted from MCF7-MMP9 cells.
The medium of the MCF7-MMP9 transfected cells, containing the secreted MMP9, was loaded onto a gelatin zymography gel. The gel was incubated overnight with N-TIMP2 proteins at a concentration of 150 nM. The white bands indicate cleavage of the gelatin by MMP9. (**A**) Untreated and N-TIMP2$_{WT}$-, C9- and C9-PEX-treated zymography gelatin gels. (**B**) Quantification of band intensity normalized to the intensity of the control (untreated) gel. Error bars represent SD. One-way ANOVA with Dunnett's multiple comparison to the untreated control was utilized for statistical analysis; ** $P < 0.005$, *** $P < 0.001$, $n = 3$. Statistical analysis for the comparison of C9-PEX to C9 was performed by Student's *t*-test, ** $P < 0.005$.

as white bands (at sizes of 92 kDa and 60 kDa for the pro- and active MMP9 isoforms, respectively [57–60]) on a dark background (Figure 3A and Supplementary Figure S6A for the cell secreted pro-MMP9 and pre-activated recombinant MMP9, respectively). As expected, all the N-TIMP2 proteins showed significant inhibitory activity against pre-activated MMP9 (60–97%, Supplementary Figure S6B) and pro-MMP9 secreted from the cells (32–95%, Figure 3B). C9-PEX exhibited the strongest inhibition of MMP9 gelatinolytic activity (~95%), despite the fact that its *Ki* for purified MMP9 was higher (i.e. lower inhibition ability) than that of C9 (Table 1). This dissonance may result from the ability of PEX, which is fused to C9 in the C9-PEX adduct, to bind to the gelatin that serves as the substrate in this assay, as previously described [61]. In addition, superior selectivity in inhibition potency of MMP9 vs MMP2 was observed for C9 (3.7-fold) and C9-PEX (6.8-fold) vs N-TIMP2$_{WT}$ (only 1.5-fold) in HT1080 cells expressing both endogenous MMPs [60] using the same zymography assay, with inhibitors at 50 nM (Supplementary Figure S7).

C9-PEX and CD44 are co-localized on the surface of MCF7-MMP9 cells

In agreement with the previously reported interactions between the PEX domain of MMP9 and CD44 [11], we observed that the multi-specific C9-PEX adduct was co-localized with CD44 on the MCF7-MMP9 cell surface (Figure 4), with both proteins clustering on the membrane. Co-localization has also been observed for MMP9 and CD44 [62], demonstrating the potential of C9-PEX for competing with MMP9 in binding to CD44. That having been said, we did not observe a significant reduction in the quantity of MMP9 upon treatment with the multi-specific C9-PEX or the mono-specific controls (Supplementary Figure S8), probably because MMP9

Biochemical Journal (2021) **478** 1139–1157
https://doi.org/10.1042/BCJ20200628

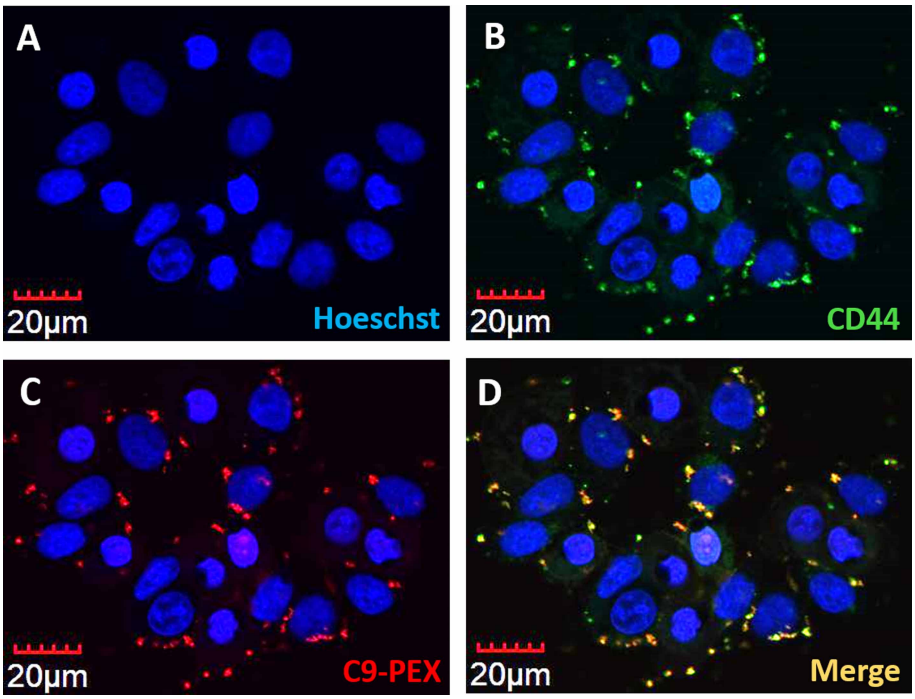

Figure 4. C9-PEX and CD44 are co-localized on the MCF7-MMP9 cell surface.

MCF7-MMP9 cells were treated with (**A**) Hoechst stain, (**B**) CD44 antibody labeled with FITC (green), or (**C**) C9-PEX labeled with DyLight 647 (red). (**D**) Merged image of panels **A** and **B**. Orange color represents co-localization and clustering of C9-PEX and CD44.

concentrations within the cells were very high, which would have made it difficult to observe small changes in MMP9 levels upon treatment with the proteins.

C9-PEX reduces the quantity of secreted MMP9

Since CD44 promotes MMP9 gene expression [14–16], we evaluated the ability of the multi-specific adduct and the mono-specific controls to reduce MMP9 levels, as reflected by the catalytic activity of cell-secreted MMP9. To this end, MCF7-MMP9 cells, expressing both CD44 and MMP9, were treated for 24 h with 1 μM N-TIMP2$_{WT}$, C9, C9-PEX, PEX, A-C9-PEX, or with C9/PEX or C9/A-C9-PEX combinations. The catalytic activity of MMP9, which reflects the quantity of MMP9 in the MCF7-MMP9 cell medium, was assayed by gelatin zymography (Figure 5). The quantity of 'free' MMP9 obtained in the assay is a function of the quantity of MMP9 that is not held in an MMP9–protein inhibitor complex and hence reflects the quantity of secreted MMP9. None of the mono-specific proteins (i.e. N-TIMP2$_{WT}$, C9, PEX or A-C9-PEX) had any effect on secreted MMP9 levels, compared with the untreated cells, but the C9-PEX adduct, the C9/PEX combination and the C9/A-C9-PEX combination significantly reduced the quantity of secreted MMP9 (~99%, ~43% and ~41%, respectively, Figure 5), with the C9-PEX adduct exhibiting the highest potency in a dose-dependent manner (Figure 6A,B). A viability assay verified that the effect on the quantity of MMP9 was not a result of the effect of C9-PEX on cell proliferation (Figure 6C). Similar results (i.e. ~88% for C9-PEX) were obtained for the human HT1080 fibrosarcoma cells, which endogenously express both MMP9 and CD44 proteins (Supplementary Figure S9).

C9-PEX generates a non-covalent, high-affinity complex with MMP9 and interferes with MMP9 dimerization

To further examine the effect of the two proteins that did have an inhibitory effect on MMP9, namely, C9 and C9-PEX, vs the protein that did not inhibit MMP9, namely, A-C9-PEX, the MCF7-MMP9 cell medium

Biochemical Journal (2021) **478** 1139–1157
https://doi.org/10.1042/BCJ20200628

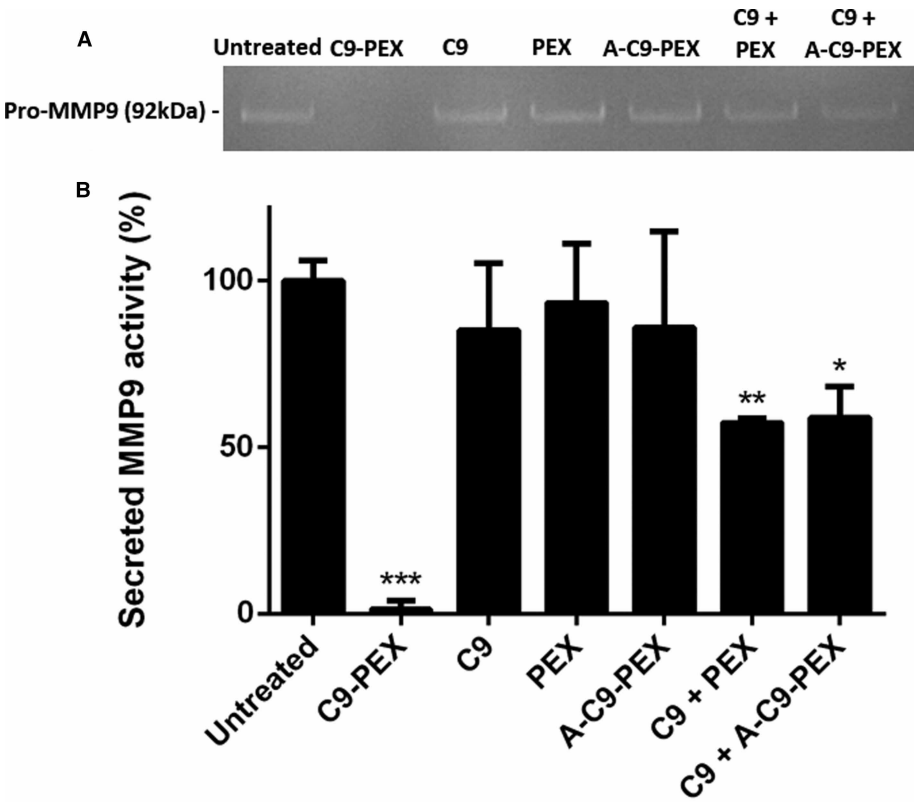

Figure 5. Effect of the proteins on the quantity of cell-secreted MMP9, as reflected by its gelatinolytic activity on gelatin SDS–PAGE.

MCF7-MMP9 cells were treated for 24 h with 1 μM of each of the proteins C9-PEX, C9, PEX or A-C9-PEX or with a combination of C9 and PEX or A-C9-PEX. The cell medium was loaded onto the gelatin zymography gel, and the intensity of the white bands, representing the amount of cell-secreted MMP9, was quantified. (**A**) Gelatin zymography gel. Lanes 2–7 represent cells treated with C9-PEX, C9, PEX, A-C9-PEX, a C9/PEX combination or a C9/A-C9-PEX combination, respectively, vs untreated cells in lane 1. All bands indicate MMP9 at 92 kDa which is indicative to its pro-enzyme (zymogen) form. (**B**) Quantification of band intensity for each treatment normalized to the intensity of the control (untreated) band. Error bars represent SD. One-way ANOVA with Dunnett's multiple comparison to the untreated control was utilized for statistical analysis; *** $P < 0.001$, ** $P < 0.01$, * $P < 0.05$, $n = 3$.

(containing cell-secreted MMP9) was incubated with C9, C9-PEX, or A-C9-PEX for 24 h. The medium was then loaded onto a gelatin zymography gel. Treatment with C9-PEX (at three different concentrations) led to a significant decrease in the quantity of MMP9, as observed from the decrease in the intensity of the white bands (Figure 7A,B). In contrast, A-C9-PEX and C9 did not have any effect on the quantity of MMP9 (Figure 7A,B). At the concentration of MMP9 used in these experiments, MMP9 homodimers were not visible on the gel, and it was therefore not possible to determine the effect of the inhibitors on MMP9 dimers. Therefore, the medium collected from MCF7-MMP9 cells was concentrated 36-fold and then treated for 24 h with C9-PEX, A-C9-PEX, C9 or a mixture of A-C9-PEX and C9. While neither the mono-inhibitors, A-C9-PEX and C9, nor the mixture of A-C9-PEX and C9 had any effect on the quantities of the MMP9 monomers or dimers, treatment with C9-PEX led to a marked decrease in both MMP9 monomers and dimers (Figure 7C). It is thus possible that C9-PEX, but not the mono-specific controls, forms a heterodimer with MMP9 by binding to the MMP9 catalytic site through C9 and to the MMP9 PEX domain through the PEX domain of the inhibitor. The C9-PEX-MMP9 heterodimer is SDS stable, similar to the MMP9 homodimer that is formed through the PEX domain. This may explain why C9-PEX, which can associate with MMP9 via two different domains, but not its mono-specific controls, interferes with MMP9 dimerization, as is shown by the reduced quantities of MMP9 homodimers in the zymography gel.

Biochemical Journal (2021) **478** 1139–1157
https://doi.org/10.1042/BCJ20200628

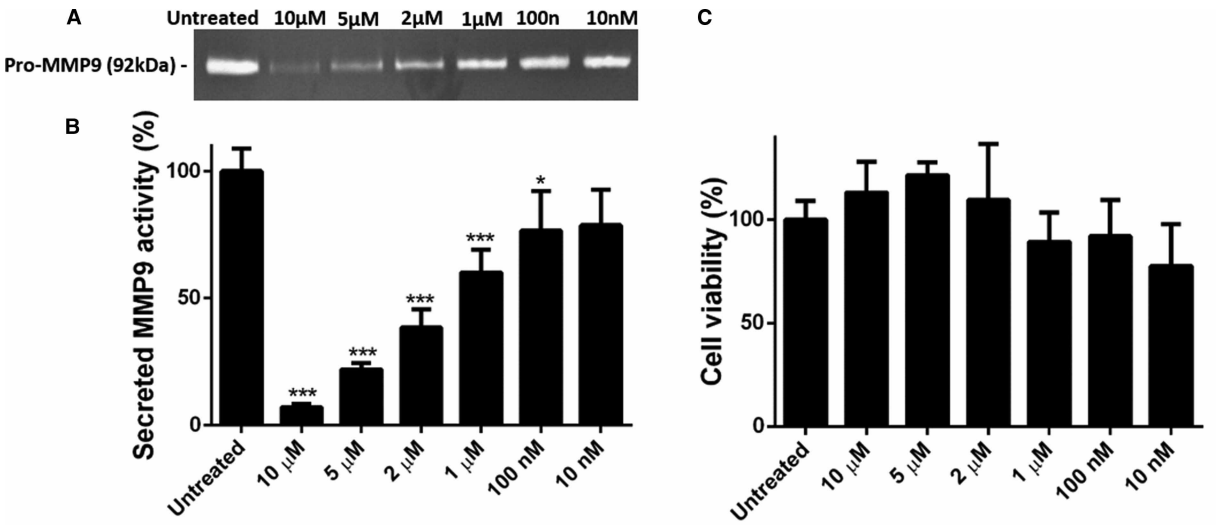

Figure 6. Effect of C9-PEX on the quantity of secreted MMP9 as determined from its gelatinolytic activity on gelatin SDS–PAGE.
MCF7-MMP9 cells were treated for 24 h with 10 nM — 10 μM of C9-PEX. The cell medium was loaded on a gelatin zymography gel, and the intensity of the white bands, representing the activity of cell-secreted MMP9, was quantified. (**A**) Gelatin zymography gel lanes 2–7 represent cells treated with 10 μM, 5 μM, 2 μM, 1 μM, 100 nM or 10 nM of C9-PEX, respectively, vs untreated cells in lane 1. (**B**) Quantification of band intensity normalized to the intensity of the control (untreated cells) band. (**C**) Cell viability assay using different concentrations of C9-PEX. The viability of the cells at each treatment concentration was normalized to the control (untreated) cells. Error bars represent SD. One-way ANOVA with Dunnett's multiple comparison to the untreated control was utilized for statistical analysis; * $P < 0.05$, *** $P < 0.001$, $n = 3$ for the zymography assay, $n = 4$ for the viability assay.

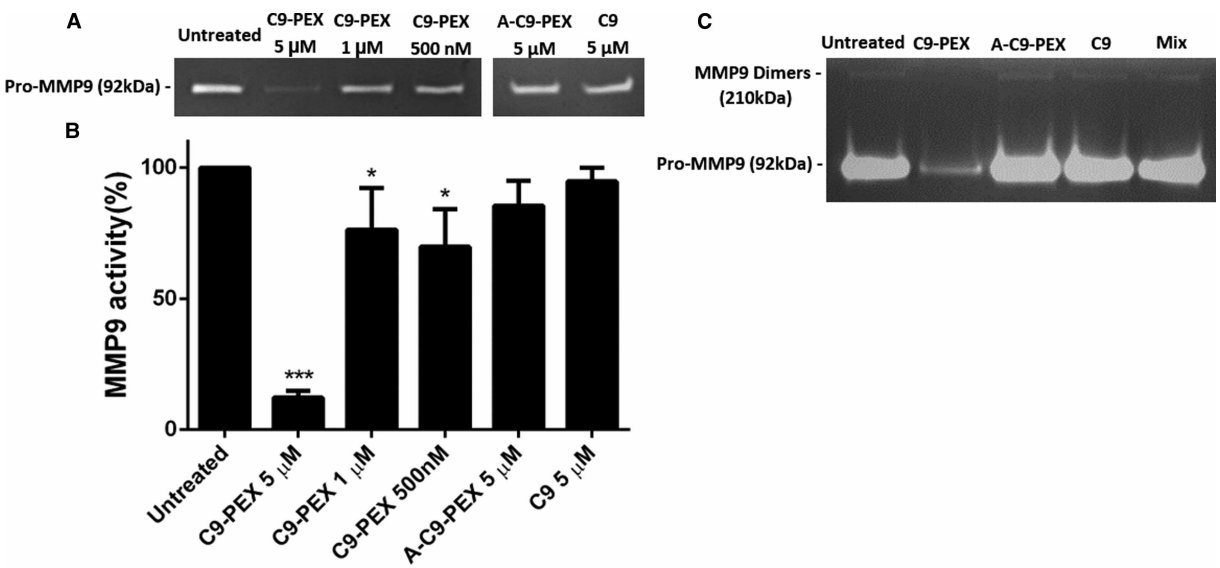

Figure 7. Effect of C9-PEX, A-C9-PEX and C9 on MMP9, as evaluated from the gelatinolytic activity of MMP9 in a gelatin SDS–PAGE assay.
MMP9 secreted from MCF7-MMP9 cells was incubated for 24 h with 500 nM — 5 μM of C9-PEX, or 5 μM of either A-C9-PEX or C9. The treated MMP9 was loaded on gelatin zymography gel, and the intensity of the white bands, representing the activity of MMP9, was quantified. (**A**) Gelatin zymography gels. Lanes 2–6 represent cells treated with 5 μM C9-PEX, 1 μM C9-PEX, 500 nM C9-PEX, 5 μM A-C9-PEX, or 5 μM C9, respectively, vs untreated cells in lane 1. (**B**) Quantification of band intensity (from panel **A**) normalized to the intensity of the control (untreated cells) band. Error bars represent SD. One-way ANOVA with Dunnett's multiple comparison to the untreated control was utilized for statistical analysis; * $P < 0.05$, *** $P < 0.0001$, $n = 3$. (**C**) Gelatin zymography gels of a concentrated MCF7-MMP9 medium. Lanes 1–5 represent untreated cells or cells treated with 5 μM of C9-PEX, A-C9-PEX, C9, or a mixture of A-C9-PEX and C9, respectively.

Biochemical Journal (2021) **478** 1139–1157
https://doi.org/10.1042/BCJ20200628

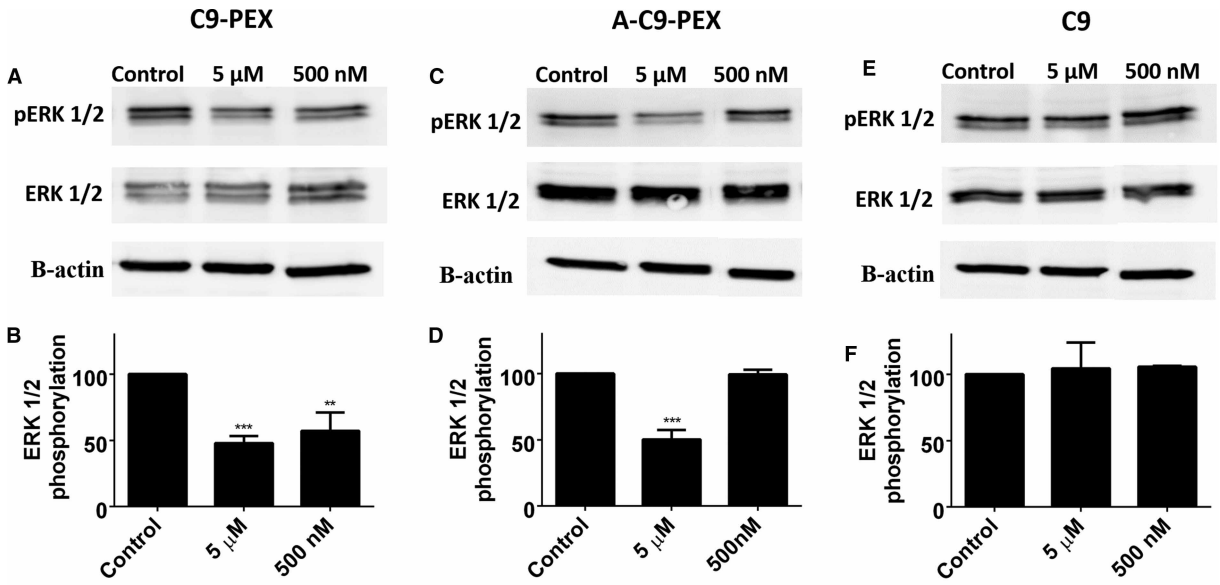

Figure 8. The PEX domain inhibits ERK1/2 phosphorylation.

MCF7-MMP9 cells were treated for 10 min with 5 μM or 500 nM of C9-PEX (**A** and **B**), A-C9-PEX (**C** and **D**) or C9 (**E** and **F**), and serum-free DMEM medium collected from MCF7-MMP9 cells pre-incubated for 24 h at 37°C (to allow secretion of MMP9). The ERK1/2 phosphorylation level was calculated by dividing the ERK1/2 phosphorylation (pERK1/2) signal intensity by the ERK1/2 signal intensity and by the control β-actin protein signal intensity. The phosphorylation of each sample was then normalized to the control, which contained samples from MCF7-MMP9 cells treated with DMEM medium collected from MCF7-MMP9 pre-incubated for 24 h at 37°C. While C9 had no effect on ERK1/2 phosphorylation, 5 μM A-C9-PEX and both 5 μM and 500 nM C9-PEX inhibited the phosphorylation. Error bars represent SD. One-way ANOVA with Dunnett's multiple comparison to the control was utilized for statistical analysis; *** $P < 0.001$, ** $P < 0.01$, $n = 3$.

The PEX domain inhibits ERK 1/2 phosphorylation

In light of reports that MMP9 homodimers induce ERK1/2 phosphorylation through the interaction of their PEX domains with CD44 [13,27], we validated the ability of the MMP9-containing medium to induce ERK 1/2 phosphorylation (Supplementary Figure S10). Thereafter, we tested the ability of C9-PEX and the mono-specific proteins C9 and A-C9-PEX to inhibit ERK1/2 phosphorylation (Figure 8). To this end, the medium from MCF7-MMP9 cells pre-incubated for 24 h in serum-free DMEM was collected. A new batch of MCF7-MMP9 cells was then treated for 10 min with this MMP-9-containing medium, supplemented with 5 μM or 500 nM of C9-PEX, C9 or A-C9-PEX. Thereafter, ERK1/2 phosphorylation was followed using western blot. As expected, when added at the high concentration, the PEX-containing proteins — both the multi-specific C9-PEX (Figure 8A,B) and the mono-specific A-C9-PEX (Figure 8C,D) — inhibited ERK1/2 phosphorylation, while C9 had no such effect (Figure 8E,F), confirming that ERK1/2 phosphorylation is mediated by PEX–CD44 interactions and not by MMP9 catalytic activity [27,38]. Of note, when the protein inhibitors were added at the low concentration, only C9-PEX exhibited significant inhibition of ERK1/2 phosphorylation.

Discussion

Extensive efforts have been made to generate potent selective inhibitors against disease-promoting MMPs, with most of them targeting the catalytic sites of MMPs. However, since the target sites share high similarity among MMP family members [43,44] and since other MMP domains and interacting molecules also affect MMP biological activity [12,61,63–65], no real progress has been reported in this endeavor. Our strategy for selective and efficient inhibition of the biological activity of MMP9 therefore focused on the three-pronged targeting of: (i) the catalytic domain of MMP9, (ii) the specific interactions between the PEX domain of MMP9, which shares low similarity within the PEX domains of all other MMP family members [66], and CD44, a receptor that is co-localized with and is functionally related to MMP9 [8,12,13], and (iii) the specific interactions

Biochemical Journal (2021) **478** 1139–1157
https://doi.org/10.1042/BCJ20200628

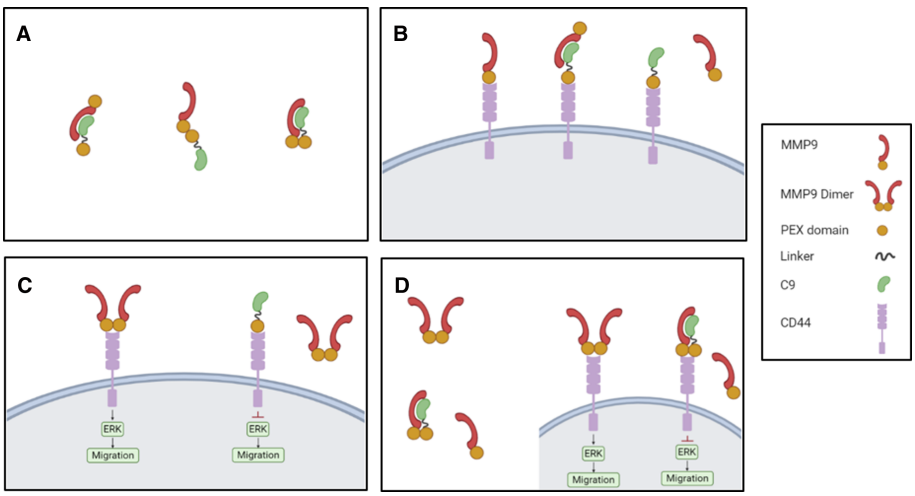

Figure 9. Schematic representation of C9-PEX's mode of inhibition.

(**A**) C9-PEX binds to the MMP9 catalytic site through C9 (left), to the PEX site through the PEX domain (middle), or to both catalytic and PEX sites (right). (**B**) MMP9 monomers dock on the cell surface via CD44 (left); this docking increases ECM degradation and cell invasiveness. C9-PEX competes with MMP9 monomers for binding to CD44 mediated via the PEX domain (right). C9-PEX can remove an MMP9 monomer from CD44 and at the same time inhibit MMP9 catalytic activity (middle). (**C**) MMP9 forms dimers through its PEX domain. The dimers, via their PEX domains, interact with CD44 and induce ERK signaling, which results in cell migration. C9-PEX can compete with MMP9 dimer binding to CD44, which will result in inhibition of ERK cell signaling. (**D**) C9-PEX can interfere with MMP9 homodimerization, and instead generate C9-PEX-MMP9 heterodimers. These heterodimers can compete with MMP9 dimers for CD44 interaction, and reduce ERK cell signaling mediated by the MMP9 dimers.

between the PEX domain of one MMP9 monomer with the same PEX domain of a different MMP9 monomer to inhibit homodimerization of MMP9 via its PEX domains.

As illustrated in Figure 9A, multi-targeting of MMP9 was achieved by generating C9-PEX, a protein adduct composed of C9 (an N-TIMP2 variant that confers enhanced activity in inhibiting the catalytic activity of MMP9) and a PEX domain that interacts with the PEX domain of MMP9. Consequently, this C9-PEX adduct was able to form a tight binding complex with MMP9, most likely by simultaneous binding both to the MMP9 catalytic pocket and to the PEX domain of MMP9. This simultaneous binding resulted in a significant increase in the affinity of C9-PEX for MMP9 and an enhancement of the ability of C9-PEX to reduce the quantities of both MMP9 monomers and homodimers *in vitro* and in cells, probably by interfering with MMP9–CD44 (Figures 5 and 6) and MMP9–MMP9 (Figure 7) interactions, respectively.

As mentioned above, MMP9 binds to CD44 through the MMP9 PEX domain, and together they dock on the cell surface (Figure 9B). This co-localization promotes ECM degradation and cancer cell invasiveness [12,18]. Antagonizing the interaction between MMP9 and CD44 is thus an important mechanism by which the C9-PEX adduct can interfere with cancer progression. MMP9 and CD44 were observed to be segregated in clusters on the cell surface [62]. This type of co-localization was also observed for C9-PEX and CD44 on MCF7-MMP9 cells (Figure 4), allowing us to posit that the multi-specific protein adduct may compete and interfere with MMP9 co-localization and interaction with CD44, thereby leading to a decrease in cell invasiveness [12]. Interestingly, it has been found that CD44 is localized at the leading edge of migrating cells [67] and that MMP9 is co-localized with CD44 on leading lamellipodial sites [62], implying that the co-localization of these two molecules is important for cell migration. In a similar manner, cell invasiveness is promoted by the catalytic activity of MMP9, which is associated with CD44 on the cell surface, as reported by Yu and Stamenkovic [12]. Their research demonstrated that the expression of CD44 on MC melanoma cells, which do not constitutively express CD44, led to an increase in invasiveness. This CD44-dependent cell invasion was inhibited by an MMP9-derived peptide inhibitor and by an anti MMP9 antibody but not by an MMP3 peptide-based inhibitor or by an isotype matched antibody [12], indicating that the catalytic activity of MMP9 promotes cell invasion only when MMP9 is associated with CD44 on the cell surface. Since MMP9 is co-localized with CD44, binding

of C9-PEX to CD44 in our system could (i) increase the local concentration of C9-PEX near both MMP9 and CD44, contributing to specificity enhancement for MMP9 inhibition, and/or (ii) enhance the accessibility of the MMP9 catalytic site for inhibition for C9 by splitting the CD44/MMP9 complex [12].

The superiority of the C9-PEX adduct over the mono-specific proteins in interfering with the MMP9–CD44 functional axis is derived from its ability to reduce MMP9 levels (Figure 5) and to attenuate ERK phosphorylation (Figure 8). Support for the potential of our adduct to interfere with MMP9–CD44 complex formation and hence to inhibit cancer progression may be drawn from a study showing that MMP9 was found in complex with CD44 on B-CLL cells but not on normal B cells, even though the normal cells also expressed both MMP9 and CD44 [11]. Notably, our designed adduct simultaneously targets two molecules that are over-expressed in cancer cells, and therefore its binding to cancer cells may be stronger than that to non-cancerous cells. Furthermore, since the CD44/MMP9 complex is formed via the binding of CD44 to the PEX domain of MMP9 on specific cells, such as B-CLL [11] and TA3 mouse mammary carcinoma [12] cells, and not in all cells that express both CD44 and MMP9 [10,11], the disruption of CD44/MMP9 complex formation by the PEX domain may be specific to those particular cell types.

In addition to its co-localization with MMP9 on the cell surface, where it is a co-receptor for MMP9, CD44 is also known to be involved in the induction of MMP9 expression via a number of different pathways, although the exact mechanisms are not known [16]. One such mechanism could be through CD44 binding to its major receptor hyaluronan, a glycosaminoglycan commonly found in the body, with the binding serving to increase MMP9 expression [16]. It is thus possible that C9-PEX binding to CD44 might interfere with hyaluronan–CD44 binding and as a result block the MMP9 expression, as has previously been shown for anti-CD44 antibodies [16]. Another pathway for CD44 involvement in MMP9 expression involves the sequential proteolytic cleavage of CD44, resulting in the formation of $CD44_{ICD}$, which translocates into the cell nucleus and promotes MMP9 gene expression [16]. Remarkably, one of the proteolytic enzymes involved in the generation of $CD44_{ICD}$ is MMP9 itself [14]. The superiority of the C9-PEX multi-specific inhibitor over its mono-specific counterparts in reducing the quantities of MMP9 when each inhibitor was added alone or in combination to MCF7-MMP9 cells (Figure 5) demonstrates that there is a synergistic effect between C9 and PEX in regulating the quantity of cell-secreted MMP9. The subsequent reduction in MMP9 levels might therefore be the result of a dual inhibition (of both MMP9 and CD44) by C9-PEX (i.e. reduction in CD44 cleavage by MMP9 [14]). Although MMP9 is a soluble protein [68], it can be localized on the cell surface through its binding to CD44 [12,66]. When MMP9 is localized on the cell surface, it might not be available for inhibition by TIMP, as previously shown for TIMP1 [12]. Thus, if we interfere with the PEX-mediated MMP9 cell surface localization and interaction with CD44 and thereby allow the C9 domain to inhibit the catalytic activity of MMP9 (now freed from CD44), then it might lead to a decrease in the formation of the $CD44_{ICD}$ cleavage product and hence to a decrease in MMP9 gene expression.

We hypothesize that the decrease in MMP9 (monomers and homodimers) levels (Figure 5) upon treatment with C9-PEX is a result of both (i) antagonizing cellular CD44 and MMP9, and (ii) generating a SDS-stable, high affinity complex with MMP9. This conclusion is based on the observations that both the C9-PEX adduct and a mixture of A-C9-PEX and C9 reduced cellular MMP9 levels (Figure 5), but only the former was able to inhibit the catalytic activity of MMP9 collected from the cell medium (Figure 7).

Another pathway that is influenced by the cross-talk between MMP9 and CD44 is ERK phosphorylation (Figure 9C). We demonstrated that high concentrations of C9-PEX and A-C9-PEX (5 μM) reduced ERK phosphorylation, but at a lower concentration (500 nM) only C9-PEX was able to inhibit ERK phosphorylation, demonstrating its superiority over the mono-specific inhibitors (Figure 8). The attenuation of ERK phosphorylation might be a result of competition of C9-PEX or A-C9-PEX with the binding of the MMP9 homodimer to CD44 (Figure 9C) or of interference with MMP9 homodimer formation (Figure 9D). Indeed, as shown in Figure 7C, the C9-PEX adduct, but not the C9 and A-C9-PEX mono-specific inhibitors, disrupts the formation of the MMP9 homodimer complex. Considering that our multi-specific protein, C9-PEX, can bind to both MMP9 and CD44, which are co-localized, C9-PEX may accumulate locally near CD44, which would allow it to compete with the MMP9 homodimer for interaction with CD44; such a mode of action would explain the superior inhibition of ERK phosphorylation by the PEX domain of C9-PEX vs the C9 and A-C9-PEX mono-specific inhibitors. As mentioned above, MMP9 homodimers are generated by non-covalent binding between two PEX domains. Since C9 does not contain the PEX domain, it is neither expected to suppress MMP9 homodimerization nor to compete with the binding of MMP9 homodimers to CD44 [27,38], and thus it will not inhibit ERK phosphorylation.

Biochemical Journal (2021) **478** 1139–1157
https://doi.org/10.1042/BCJ20200628

Finally, we touch on a subject that was mentioned in brief in the Introduction. It is known that the CD44/MMP9 complex formed on the cell surface leads to ECM degradation and to the migration, invasion and metastasis of cancer cells [11,18,25,26], and some years ago it was also suggested that the formation of this complex induces the activation of TGF-β, thereby promoting tumor growth and invasiveness [12]. Nevertheless, despite many years of intense study, it is still not known how the CD44, MMP-9 and TGF-β triad controls the proliferation, survival, activation, and differentiation of B cells or the development and functions of innate cells, including natural killer cells, macrophages, dendritic cells, and granulocytes. In conclusion, by simultaneously targeting two co-localized and functionally related molecules — MMP9 and CD44 — we were able to engineer an inhibitor of neoplasia that is both potent and specific. In view of the similarity between the active sites of the different MMPs, this method of targeting of a particular MMP and its co-localized, functionally related receptor, can be applied to other MMP family members as platform for generating better specificity and enhanced antagonism and hence for the creation of new-generation therapeutics for cancer and other diseases.

Competing Interests

The authors declare that there are no competing interests associated with the manuscript.

Funding

This work was supported by the Israel Science Foundation [grant number 615/14] to N.P.

Open Access Statement

Open access for this article was enabled by the participation of Ben-Gurion University of The Negev in an all-inclusive Read & Publish pilot with Portland Press and the Biochemical Society under a transformative agreement with MALMAD.

CRediT Contribution

Niv Papo: Conceptualization, Resources, Formal analysis, Supervision, Funding acquisition, Validation, Investigation, Writing — original draft, Project administration, Writing — review and editing. **Gal Yosef:** Conceptualization, Data curation, Formal analysis, Validation, Investigation, Methodology, Writing — original draft, Writing — review and editing. **Hezi Hayun:** Data curation, Formal analysis, Writing — review and editing.

Acknowledgements

The authors thank Dr. Alon Zilka and Dr. Uzi Hadad for their technical assistance. FACS experiments were performed at the Ilse Katz Institute for Nanoscale Science and Technology, BGU. Confocal microscopy experiments were performed at the NIBN proteomics unit, BGU.

Abbreviations

B-CLL, B-cell chronic lymphocytic leukemia; BGU, Ben-Gurion University of the Negev; BSA, bovine serum albumin; $CD44_{ICD}$, intracytoplasmic domain of CD44; DMEM, Dulbecco's modified Eagle's medium; ECM, extracellular matrix; ERK, extracellular signal-regulated kinase; FACS, fluorescence-activated cell sorting; MMP, matrix metalloproteinase; PE, phycoerythrin; PEX, hemopexin domain of MMP9; RPMI, Roswell Park Memorial Institute; TGF-β, transforming growth factor beta; TIMP, tissue inhibitor of matrix metalloproteinase; YSD, yeast surface display.

References

1 Mackay, C.R., Terpe, H.J., Stauder, R., Marston, W.L., Stark, H. and Gunthert, U. (1994) Expression and modulation of CD44 variant isoforms in humans. *J. Cell Biol.* **124**, 71–82 https://doi.org/10.1083/jcb.124.1.71

2 Chen, C., Zhao, S., Karnad, A. and Freeman, J.W. (2018) The biology and role of CD44 in cancer progression: therapeutic implications. *J. Hematol. Oncol.* **11**, 64 https://doi.org/10.1186/s13045-018-0605-5

3 Motohara, T., Fujimoto, K., Tayama, S., Narantuya, D., Sakaguchi, I., Tashiro, H. et al. (2016) CD44 variant 6 as a predictive biomarker for distant metastasis in patients with epithelial ovarian cancer. *Obstet. Gynecol.* **127**, 1003–1011 https://doi.org/10.1097/AOG.0000000000001420

4 Franzmann, E.J., Reategui, E.P., Pedroso, F., Pernas, F.G., Karakullukcu, B.M., Carraway, K.L. et al. (2007) Soluble CD44 is a potential marker for the early detection of head and neck cancer. *Cancer Epidemiol. Biomarkers Prev.* **16**, 1348–1355 https://doi.org/10.1158/1055-9965.EPI-06-0011

5 Hirata, K., Suzuki, H., Imaeda, H., Matsuzaki, J., Tsugawa, H., Nagano, O. et al. (2013) CD44 variant 9 expression in primary early gastric cancer as a predictive marker for recurrence. *Br. J. Cancer* **109**, 379–386 https://doi.org/10.1038/bjc.2013.314

6 Luo, Y. and Tan, Y. (2016) Prognostic value of CD44 expression in patients with hepatocellular carcinoma: meta-analysis. *Cancer Cell Int.* **16**, 47 https://doi.org/10.1186/s12935-016-0325-2
7 Liu, Y., Wu, T., Lu, D., Zhen, J. and Zhang, L. (2018) CD44 overexpression related to lymph node metastasis and poor prognosis of pancreatic cancer. *Int. J. Biol. Markers* **33**, 308–313 https://doi.org/10.1177/1724600817746951
8 Turley, E.A. and Naor, D. (2012) RHAMM and CD44 peptides-analytic tools and potential drugs. *Front. Biosci. (Landmark Ed.)* **17**, 1775–1794 https://doi.org/10.2741/4018
9 Nagase, H., Visse, R. and Murphy, G. (2006) Structure and function of matrix metalloproteinases and TIMPs. *Cardiovasc. Res.* **69**, 562–573 https://doi.org/10.1016/j.cardiores.2005.12.002
10 Stamenkovic, I. (2000) Matrix metalloproteinases in tumor invasion and metastasis. *Semin. Cancer Biol.* **10**, 415–433 https://doi.org/10.1006/scbi.2000.0379
11 Redondo-Munoz, J., Ugarte-Berzal, E., Garcia-Marco, J.A., del Cerro, M.H., Van den Steen, P.E., Opdenakker, G. et al. (2008) Alpha4beta1 integrin and 190-kDa CD44v constitute a cell surface docking complex for gelatinase B/MMP-9 in chronic leukemic but not in normal B cells. *Blood* **112**, 169–178 https://doi.org/10.1182/blood-2007-08-109249
12 Yu, Q. and Stamenkovic, I. (1999) Localization of matrix metalloproteinase 9 to the cell surface provides a mechanism for CD44-mediated tumor invasion. *Genes Dev.* **13**, 35–48 https://doi.org/10.1101/gad.13.1.35
13 Bauvois, B. (2012) New facets of matrix metalloproteinases MMP-2 and MMP-9 as cell surface transducers: outside-in signaling and relationship to tumor progression. *Biochim. Biophys. Acta* **1825**, 29–36 https://doi.org/10.1016/j.bbcan.2011.10.001
14 Chetty, C., Vanamala, S.K., Gondi, C.S., Dinh, D.H., Gujrati, M. and Rao, J.S. (2012) MMP-9 induces CD44 cleavage and CD44 mediated cell migration in glioblastoma xenograft cells. *Cell. Signal.* **24**, 549–559 https://doi.org/10.1016/j.cellsig.2011.10.008
15 Senbanjo, L.T., AlJohani, H., Majumdar, S. and Chellaiah, M.A. (2019) Characterization of CD44 intracellular domain interaction with RUNX2 in PC3 human prostate cancer cells. *Cell Commun. Signal.* **17**, 80 https://doi.org/10.1186/s12964-019-0395-6
16 Miletti-Gonzalez, K.E., Murphy, K., Kumaran, M.N., Ravindranath, A.K., Wernyj, R.P., Kaur, S., et al. (2012) Identification of function for CD44 intracytoplasmic domain (CD44-ICD): modulation of matrix metalloproteinase 9 (MMP-9) transcription via novel promoter response element. *J. Biol. Chem.* **287**, 18995–19007 https://doi.org/10.1074/jbc.M111.318774
17 Ramos-DeSimone, N., Hahn-Dantona, E., Sipley, J., Nagase, H., French, D.L. and Quigley, J.P. (1999) Activation of matrix metalloproteinase-9 (MMP-9) via a converging plasmin/stromelysin-1 cascade enhances tumor cell invasion. *J. Biol. Chem.* **274**, 13066–13076 https://doi.org/10.1074/jbc.274.19.13066
18 Yu, Q. and Stamenkovic, I. (2000) Cell surface-localized matrix metalloproteinase-9 proteolytically activates TGF-beta and promotes tumor invasion and angiogenesis. *Genes Dev.* **14**, 163–176 PMID:10652271
19 Sternlicht, M.D. and Werb, Z. (2001) How matrix metalloproteinases regulate cell behavior. *Annu. Rev. Cell Dev. Biol.* **17**, 463–516 https://doi.org/10.1146/annurev.cellbio.17.1.463
20 Loffek, S., Schilling, O. and Franzke, C.-W. (2011) Biological role of matrix metalloproteinases: a critical balance. *Eur. Respir. J.* **38**, 191–208 https://doi.org/10.1183/09031936.00146510
21 Ranuncolo, S.M., Armanasco, E., Cresta, C., Bal De Kier Joffe, E. and Puricelli, L. (2003) Plasma MMP-9 (92 kDa-MMP) activity is useful in the follow-up and in the assessment of prognosis in breast cancer patients. *Int. J. Cancer* **106**, 745–751 https://doi.org/10.1002/ijc.11288
22 Lengyel, E., Schmalfeldt, B., Konik, E., Spathe, K., Harting, K., Fenn, A., et al. (2001) Expression of latent matrix metalloproteinase 9 (MMP-9) predicts survival in advanced ovarian cancer. *Gynecol. Oncol.* **82**, 291–298 https://doi.org/10.1006/gyno.2001.6243
23 Reis, S.T., Leite, K.R.M., Piovesan, L.F., Pontes-Junior, J., Viana, N.I., Abe, D.K., et al. (2012) Increased expression of MMP-9 and IL-8 are correlated with poor prognosis of bladder cancer. *BMC Urol.* **12**, 18 https://doi.org/10.1186/1471-2490-12-18
24 Huang, H. (2018) Matrix metalloproteinase-9 (MMP-9) as a cancer biomarker and MMP-9 biosensors: recent advances. *Sensors (Basel)* **18**, 3249 https://doi.org/10.3390/s18103249
25 Bourguignon, L.Y., Gunja-Smith, Z., Iida, N., Zhu, H.B., Young, L.J., Muller, W.J. et al. (1998) CD44v(3,8-10) is involved in cytoskeleton-mediated tumor cell migration and matrix metalloproteinase (MMP-9) association in metastatic breast cancer cells. *J. Cell. Physiol.* **176**, 206–215 https://doi.org/10.1002/(SICI)1097-4652(199807)176:1<206::AID-JCP22>3.0.CO;2-3
26 Desai, B., Rogers, M.J. and Chellaiah, M.A. (2007) Mechanisms of osteopontin and CD44 as metastatic principles in prostate cancer cells. *Mol. Cancer* **6**, 18 https://doi.org/10.1186/1476-4598-6-18
27 Dufour, A., Zucker, S., Sampson, N.S., Kuscu, C. and Cao, J. (2010) Role of matrix metalloproteinase-9 dimers in cell migration: design of inhibitory peptides. *J. Biol. Chem.* **285**, 35944–35956 https://doi.org/10.1074/jbc.M109.091769
28 Marshall, D.C., Lyman, S.K., McCauley, S., Kovalenko, M., Spangler, R., Liu, C., et al. (2015) Selective allosteric inhibition of MMP9 is efficacious in preclinical models of ulcerative colitis and colorectal cancer. *PLoS ONE* **10**, e0127063 https://doi.org/10.1371/journal.pone.0127063
29 Owyong, M., Chou, J., van den Bijgaart, R.J., Kong, N., Efe, G., Maynard, C., et al. (2019) MMP9 modulates the metastatic cascade and immune landscape for breast cancer anti-metastatic therapy. *Life Sci. Alliance* **2**, e201800226 https://doi.org/10.26508/lsa.201800226
30 Seiter, S., Arch, R., Reber, S., Komitowski, D., Hofmann, M., Ponta, H. et al. (1993) Prevention of tumor metastasis formation by anti-variant CD44. *J. Exp. Med.* **177**, 443–455 https://doi.org/10.1084/jem.177.2.443
31 Orian-Rousseau, V. (2010) CD44, a therapeutic target for metastasising tumours. *Eur. J. Cancer* **46**, 1271–1277 https://doi.org/10.1016/j.ejca.2010.02.024
32 Orian-Rousseau, V. and Ponta, H. (2015) Perspectives of CD44 targeting therapies. *Arch. Toxicol.* **89**, 3–14 https://doi.org/10.1007/s00204-014-1424-2
33 Lauer-Fields, J.L., Whitehead, J.K., Li, S., Hammer, R.P., Brew, K. and Fields, G.B. (2008) Selective modulation of matrix metalloproteinase 9 (MMP-9) functions via exosite inhibition. *J. Biol. Chem.* **283**, 20087–20095 https://doi.org/10.1074/jbc.M801438200
34 Scannevin, R.H., Alexander, R., Haarlander, T.M., Burke, S.L., Singer, M., Huo, C., et al. (2017) Discovery of a highly selective chemical inhibitor of matrix metalloproteinase-9 (MMP-9) that allosterically inhibits zymogen activation. *J. Biol. Chem.* **292**, 17963–17974 https://doi.org/10.1074/jbc.M117.806075

Biochemical Journal (2021) **478** 1139–1157
https://doi.org/10.1042/BCJ20200628

35 Liu, L.-K. and Finzel, B.C. (2014) Fragment-based identification of an inducible binding site on cell surface receptor CD44 for the design of protein-carbohydrate interaction inhibitors. *J. Med. Chem.* **57**, 2714–2725 https://doi.org/10.1021/jm5000276

36 Ugarte-Berzal, E., Bailon, E., Amigo-Jimenez, I., Albar, J.P., Garcia-Marco, J.A. and Garcia-Pardo, A. (2014) A novel CD44-binding peptide from the pro-matrix metalloproteinase-9 hemopexin domain impairs adhesion and migration of chronic lymphocytic leukemia (CLL) cells. *J. Biol. Chem.* **289**, 15340–15349 https://doi.org/10.1074/jbc.M114.559187

37 Roderfeld, M., Wagner, S., Henkel, C., Grötzinger, J. and Roeb, E. (2007) MMP-9-hemopexin domain hampers adhesion and migration of colorectal cancer cells. *Int. J. Oncol* **30**, 985–992 https://doi.org/10.3892/ijo.30.4.985

38 Dufour, A., Sampson, N.S., Li, J., Kuscu, C., Rizzo, R.C., Deleon, J.L., et al. (2011) Small-molecule anticancer compounds selectively target the hemopexin domain of matrix metalloproteinase-9. *Cancer Res.* **71**, 4977–4988 https://doi.org/10.1158/0008-5472.CAN-10-4552

39 Brew, K. and Nagase, H. (2010) The tissue inhibitors of metalloproteinases (TIMPs): an ancient family with structural and functional diversity. *Biochim. Biophys. Acta* **1803**, 55–71 https://doi.org/10.1016/j.bbamcr.2010.01.003

40 Arkadash, V., Yosef, G., Shirian, J., Cohen, I., Horev, Y., Grossman, M. et al. (2017) Development of high affinity and high specificity inhibitors of matrix metalloproteinase 14 through computational design and directed evolution. *J. Biol. Chem.* **292**, 3481–3495 https://doi.org/10.1074/jbc.M116.756718

41 Folgueras, A.R., Pendas, A.M., Sanchez, L.M. and Lopez-Otin, C. (2004) Matrix metalloproteinases in cancer: from new functions to improved inhibition strategies. *Int. J. Dev. Biol.* **48**, 411–424 https://doi.org/10.1387/ijdb.041811af

42 Decock, J., Thirkettle, S., Wagstaff, L. and Edwards, D.R. (2011) Matrix metalloproteinases: protective roles in cancer. *J. Cell. Mol. Med.* **15**, 1254–1265 https://doi.org/10.1111/j.1582-4934.2011.01302.x

43 Overall, C.M. and Kleifeld, O. (2006) Towards third generation matrix metalloproteinase inhibitors for cancer therapy. *Br. J. Cancer* **94**, 941–946 https://doi.org/10.1038/sj.bjc.6603043

44 Vandenbroucke, R.E. and Libert, C. (2014) Is there new hope for therapeutic matrix metalloproteinase inhibition? *Nat. Rev. Drug Discov.* **13**, 904–927 https://doi.org/10.1038/nrd4390

45 Itoh, Y. and Seiki, M. (2004) MT1-MMP: an enzyme with multidimensional regulation. *Trends Biochem. Sci.* **29**, 285–289 https://doi.org/10.1016/j.tibs.2004.04.001

46 Deryugina, E.I., Ratnikov, B., Monosov, E., Postnova, T.I., DiScipio, R., Smith, J.W. et al. (2001) MT1-MMP initiates activation of pro-MMP-2 and integrin alphavbeta3 promotes maturation of MMP-2 in breast carcinoma cells. *Exp. Cell Res.* **263**, 209–223 https://doi.org/10.1006/excr.2000.5118

47 Toth, M., Chvyrkova, I., Bernardo, M.M., Hernandez-Barrantes, S. and Fridman, R. (2003) Pro-MMP-9 activation by the MT1-MMP/MMP-2 axis and MMP-3: role of TIMP-2 and plasma membranes. *Biochem. Biophys. Res. Commun.* **308**, 386–395 https://doi.org/10.1016/S0006-291X(03)01405-0

48 Fernandez-Catalan, C., Bode, W., Huber, R., Turk, D., Calvete, J.J., Lichte, A. et al. (1998) Crystal structure of the complex formed by the membrane type 1-matrix metalloproteinase with the tissue inhibitor of metalloproteinases-2, the soluble progelatinase A receptor. *EMBO J.* **17**, 5238–5248 https://doi.org/10.1093/emboj/17.17.5238

49 Boder, E.T. and Wittrup, K.D. (2000) Yeast surface display for directed evolution of protein expression, affinity, and stability. *Methods Enzymol.* **328**, 430–444 https://doi.org/10.1016/S0076-6879(00)28410-3

50 Cha, H., Kopetzki, E., Huber, R., Lanzendorfer, M. and Brandstetter, H. (2002) Structural basis of the adaptive molecular recognition by MMP9. *J. Mol. Biol.* **320**, 1065–1079 https://doi.org/10.1016/S0022-2836(02)00558-2

51 Rowsell, S., Hawtin, P., Minshull, C.A., Jepson, H., Brockbank, S.M.V., Barratt, D.G., et al. (2002) Crystal structure of human MMP9 in complex with a reverse hydroxamate inhibitor. *J. Mol. Biol.* **319**, 173–181 https://doi.org/10.1016/S0022-2836(02)00262-0

52 Yosef, G., Arkadash, V. and Papo, N. (2018) Targeting the MMP-14/MMP-2/integrin alphavbeta3 axis with multispecific N-TIMP2-based antagonists for cancer therapy. *J. Biol. Chem.* **293**, 13310–13326 https://doi.org/10.1074/jbc.RA118.004406

53 Frankowski, H., Gu, Y.-H., Heo, J.H., Milner, R. and Del Zoppo, G.J. (2012) Use of gel zymography to examine matrix metalloproteinase (gelatinase) expression in brain tissue or in primary glial cultures. *Methods Mol. Biol.* **814**, 221–233 https://doi.org/10.1007/978-1-61779-452-0_15

54 Shirian, J., Arkadash, V., Cohen, I., Sapir, T., Radisky, E.S., Papo, N. et al. (2018) Converting a broad matrix metalloproteinase family inhibitor into a specific inhibitor of MMP-9 and MMP-14. *FEBS Lett.* **592**, 1122–1134 https://doi.org/10.1002/1873-3468.13016

55 Fernandez, C.A., Butterfield, C., Jackson, G. and Moses, M.A. (2003) Structural and functional uncoupling of the enzymatic and angiogenic inhibitory activities of tissue inhibitor of metalloproteinase-2 (TIMP-2): loop 6 is a novel angiogenesis inhibitor. *J. Biol. Chem.* **278**, 40989–40995 https://doi.org/10.1074/jbc.M306176200

56 Wingfield, P.T., Sax, J.K., Stahl, S.J., Kaufman, J., Palmer, I., Chung, V. et al. (1999) Biophysical and functional characterization of full-length, recombinant human tissue inhibitor of metalloproteinases-2 (TIMP-2) produced in *Escherichia coli*. Comparison of wild type and amino-terminal alanine appended variant with implications for the mechanism of TIMP functions. *J. Biol. Chem.* **274**, 21362–21368 https://doi.org/10.1074/jbc.274.30.21362

57 Vandooren, J., Geurts, N., Martens, E., Van den Steen, P.E. and Opdenakker, G. (2013) Zymography methods for visualizing hydrolytic enzymes. *Nat. Methods* **10**, 211 https://doi.org/10.1038/nmeth.2371

58 Min, D., Moore, A.G., Bain, M.A., Breit, S.N. and Lyons, J.G. (2002) Activation of macrophage promatrix metalloproteinase-9 by lipopolysaccharide-associated proteinases. *J. Immunol.* **168**, 2449–2455 https://doi.org/10.4049/jimmunol.168.5.2449

59 Gong, Y., Hart, E., Shchurin, A. and Hoover-Plow, J. (2008) Inflammatory macrophage migration requires MMP-9 activation by plasminogen in mice. *J. Clin. Invest.* **118**, 3012–3024 https://doi.org/10.1172/JCI32750

60 Toth, M. and Fridman, R. (2001) Assessment of gelatinases (MMP-2 and MMP-9) by gelatin zymography. *Methods Mol. Med.* **57**, 163–174 https://doi.org/10.1385/1-59259-136-1:163

61 Roeb, E., Schleinkofer, K., Kernebeck, T., Potsch, S., Jansen, B., Behrmann, I. et al. (2002) The matrix metalloproteinase 9 (mmp-9) hemopexin domain is a novel gelatin binding domain and acts as an antagonist. *J. Biol. Chem.* **277**, 50326–50332 https://doi.org/10.1074/jbc.M207446200

62 Abecassis, I., Olofsson, B., Schmid, M., Zalcman, G. and Karniguian, A. (2003) RhoA induces MMP-9 expression at CD44 lamellipodial focal complexes and promotes HMEC-1 cell invasion. *Exp. Cell Res.* **291**, 363–376 https://doi.org/10.1016/j.yexcr.2003.08.006

63 Stefanidakis, M. and Koivunen, E. (2006) Cell-surface association between matrix metalloproteinases and integrins: role of the complexes in leukocyte migration and cancer progression. *Blood* **108**, 1441–1450 https://doi.org/10.1182/blood-2006-02-005363

64 Brooks, P.C., Strömblad, S., Sanders, L.C., von Schalscha, T.L., Aimes, R.T., Stetler-Stevenson, W.G. et al. (1996) Localization of matrix metalloproteinase MMP-2 to the surface of invasive cells by interaction with integrin alpha v beta 3. *Cell* **85**, 683–693 https://doi.org/10.1016/S0092-8674(00)81235-0

65 Brooks, P.C., Silletti, S., von Schalscha, T.L., Friedlander, M. and Cheresh, D.A. (1998) Disruption of angiogenesis by PEX, a noncatalytic metalloproteinase fragment with integrin binding activity. *Cell* **92**, 391–400 https://doi.org/10.1016/S0092-8674(00)80931-9

66 Adhipandito, C.F., Putri, D., Sari, K., Aprilianto, E. and Jenie, R.I. (2019) Matrix metalloproteinase9 as the protein target in anti-breast cancer drug discovery: an approach by targeting hemopexin domain. *Futur. J. Pharm. Sci.* **1**, 1–15 https://doi.org/10.1186/s43094-019-0001-1

67 Suenaga, N., Mori, H., Itoh, Y. and Seiki, M. (2005) CD44 binding through the hemopexin-like domain is critical for its shedding by membrane-type 1 matrix metalloproteinase. *Oncogene* **24**, 859–868 https://doi.org/10.1038/sj.onc.1208258

68 Visse, R. and Nagase, H. (2003) Matrix metalloproteinases and tissue inhibitors of metalloproteinases: structure, function, and biochemistry. *Circ. Res.* **92**, 827–839 https://doi.org/10.1161/01.RES.0000070112.80711.3D